NPP2020, Moscow, 16.12.2020

Pressure-Produced Ionization of Nonideal Degenerate Plasmas and Electrical Conductivity

G. Röpke, H.Reinholz
Universität Rostock

Pressure-Produced Ionization of Nonideal Degenerate Plasmas and Electrical Conductivity

Journal of Experimental and Theoretical Physics, Vol. 97, No. 2, 2003, pp. 259–278.
Translated from Zhurnal Éksperimental'noĭ i Teoreticheskoĭ Fiziki, Vol. 124, No. 2, 2003, pp. 288–309.

PLASMA, GASES

Pressure-Produced Ionization of Nonideal Plasma in a Megabar Range of Dynamic Pressures

V. E. Fortov[a], V. Ya. Ternovoĭ[a], M. V. Zhernokletov[b], M. A. Mochalov[b], A. L. Mikhailov[b], A. S. Filimonov[a], A. A. Pyalling[a], V. B. Mintsev[a,*], V. K. Gryaznov[a,], and I. L. Iosilevskiĭ[c]**

Phase diagram of Hydrogen

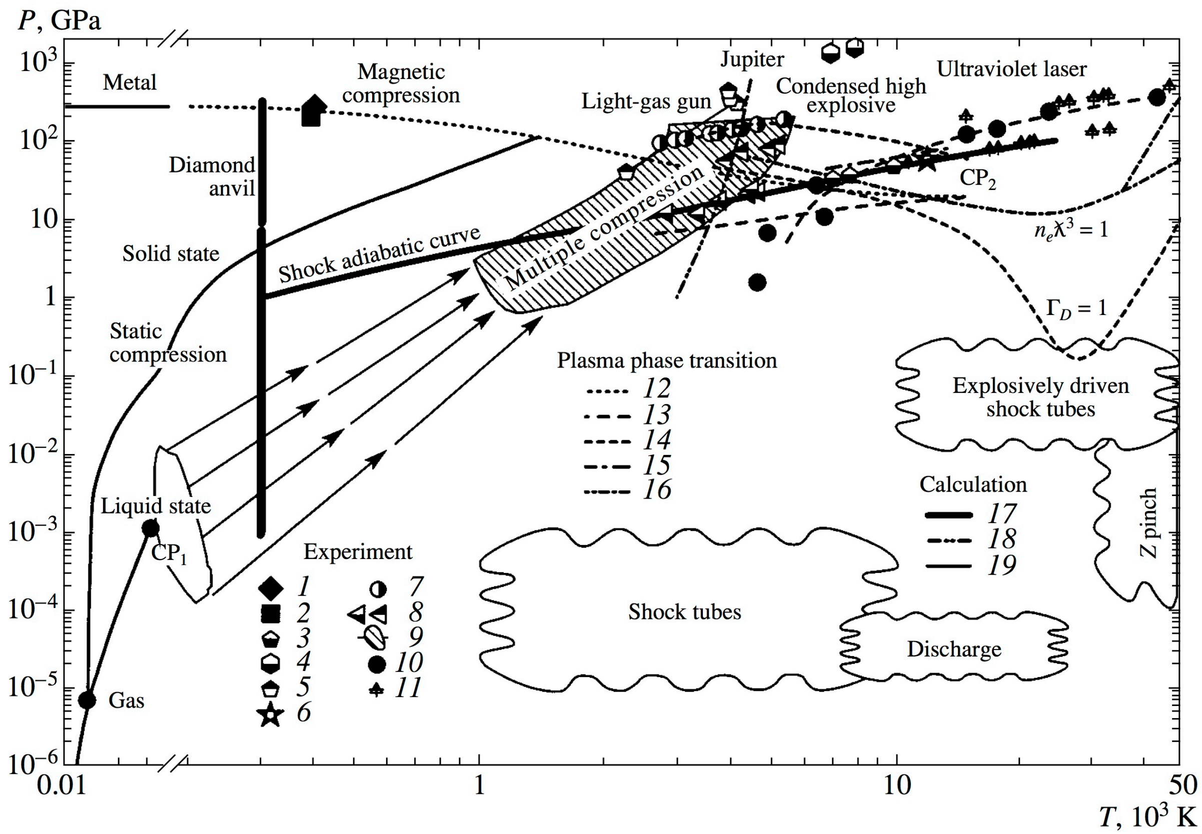

Fig. 1. Phase diagram of hydrogen. The displayed experimental data were obtained in (*1*, *2*) magnetic compression [29, 30], (*3*) *Z* pinch [33], (*4*, *5*) cylindrical compression [26, 27], (*6*) spherical compression [28]; (*7*, *8*) single and multiple compression by means of a light-gas gun [34, 35], (*9*) multiple shock compression [36], and (*10*, *11*) shock compression by a laser [31, 32]. The estimates for the critical point of the plasma phase transition in hydrogen were taken from the articles of (*12*) Beule *et al*. [37], (*13*) Robnic and Kundt [38], (*14*) Saumon and Chabrier [23], (*15*) Haronska *et al*. [39], and (*16*) Mulenko *et al*. [24]. The calculated data correspond to (*17*) compression at a diamond anvil [11], (*18*) the parameters of Jupiter's atmosphere [40], and (*19*) the adiabatic curve for the shock compression of hydrogen [34].

V. E. Fortov *et al*., J. Exp. Theor. Phys. **97**, 259 (2003)

Electrical conductivity of Hydrogen

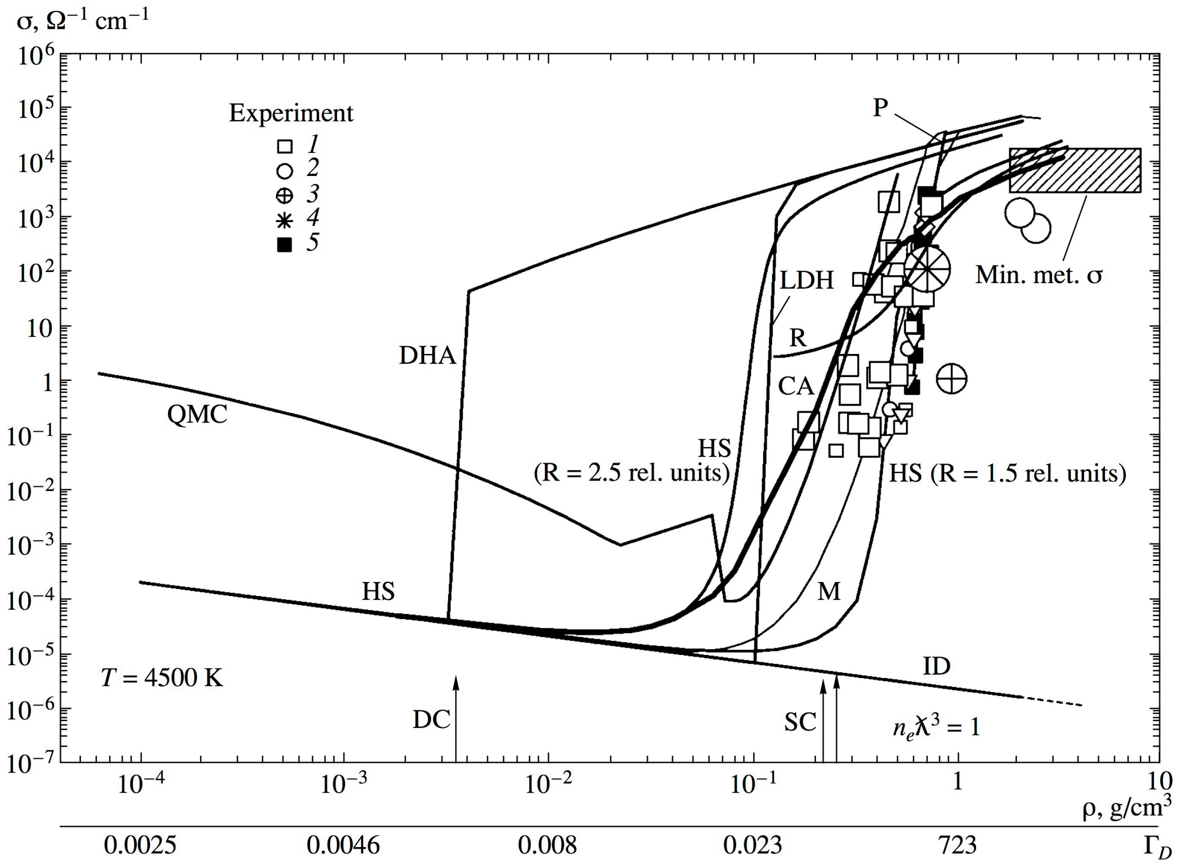

Fig. 7. Electrical conductivity of hydrogen as a function of density. The experimental data of the present study were obtained for (*1*) planar systems and (*2*) cylindrical systems. The remaining data were borrowed from (*3*) [29] and (*4*) [30] (magnetic compression) and from (*5*) [35] (experiments with light-gas guns).

V. E. Fortov *et al.*, J. Exp. Theor. Phys. **97**, 259 (2003)

Electron degeneracy: Θ=T/T$_F$

5. ELECTRICAL CONDUCTIVITY OF NONIDEAL PLASMAS

In order to describe the electrical conductivity over a broad range of parameters where electrons may obey either Boltzmann or Fermi statistics, expressions (3.1)–(3.4) were combined into an interpolation expression within the τ approximation [94]; that is,

$$\sigma = \frac{4e^2(k_BT)^{-3/2}}{3\sqrt{\pi}m_e}\frac{2}{\lambda_e^2}\int_0^\infty \varepsilon^{3/2}\tau(\varepsilon)\left(-\frac{\partial f_0}{\partial \varepsilon}\right)d\varepsilon, \qquad (5.1)$$

where f_0 is the electron distribution; τ is the relaxation time,

$$\tau^{-1}(\varepsilon) = \sqrt{\frac{2\varepsilon}{m_e}}\left[\sum_j \gamma_j n_j Q_{ej}(\varepsilon) + n_a Q_{ea}(\varepsilon)\right],$$

Q_{ea} and Q_{ei} are the transport cross sections for, respectively, electron–atom and electron–ion scattering; and γ_j is a correction for electron–electron scattering. For the case where the change in statistics occurs, this correction was interpolated as [22]

$$\gamma_j = \gamma_j^B - (\gamma_j^B - 1)\frac{T_F}{\sqrt{T_F^2 + T^2}}$$

with T_F being the Fermi temperature and γ_j^B is a correction for the Boltzmann plasma.

V. E. Fortov *et al*., J. Exp. Theor. Phys. **97**, 259 (2003)

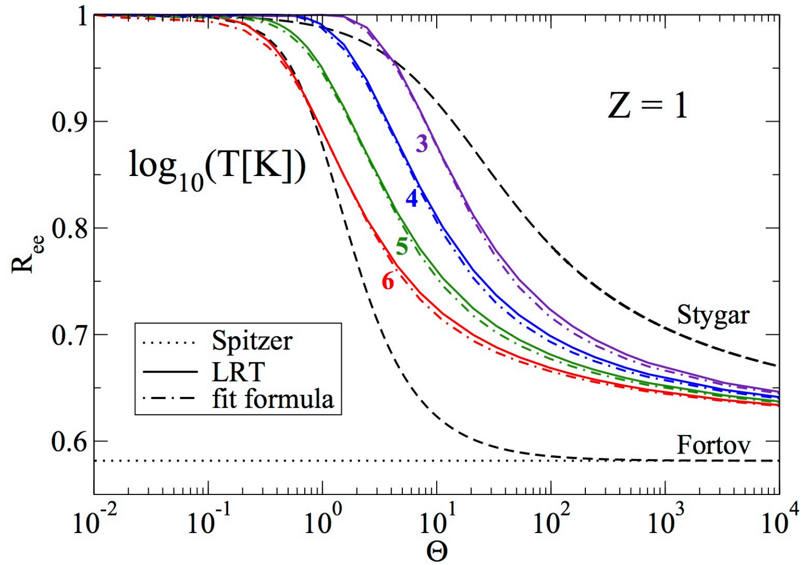

FIG. 1. (Color online) Correction factor R_{ee} of the conductivity due to e-e collisions as function of degeneracy parameter Θ at $Z = 1$ for different temperatures $T = (10^3, 10^4, 10^5, 10^6)$ K. Numerical calculations (LRT, full lines) are compared with the fit formula (34) (dot-dashed lines) and the approximations (40) of Stygar *et al.* [11] and (41) of Fortov *et al.* [12] (dashed lines).

and Fortov *et al.* [12],

$$R_{ee}^{\mathrm{Fortov}}(\Theta, Z) = R_{ee}^{\mathrm{KT}}(Z) + \frac{1 - R_{ee}^{\mathrm{KT}}(Z)}{\sqrt{1+\Theta^2}}, \qquad (41)$$

with the Spitzer values $R_{ee}^{\mathrm{KT}}(Z=1) = 0.582$, see Eq. (29),

H. Reinholz *et al*., Phys. Rev. E **91**, 043105 (2015).

Outline

- Ionization potential depression: Steward-Pyatt (SP) and improvements: ionic structure factor, degeneracy
- Density functional theory (DFT-MD) calculations, frequency-dependent conductivity
- Electrical conductivity, generalized linear response theory
- Kubo-Greenwood formula
- Electrical conductivity of partially ionized plasma

NIF XRTS experiments find higher carbon K-shell ionization than predicted by widely used IPD models (Stewart & Pyatt, OPAL)

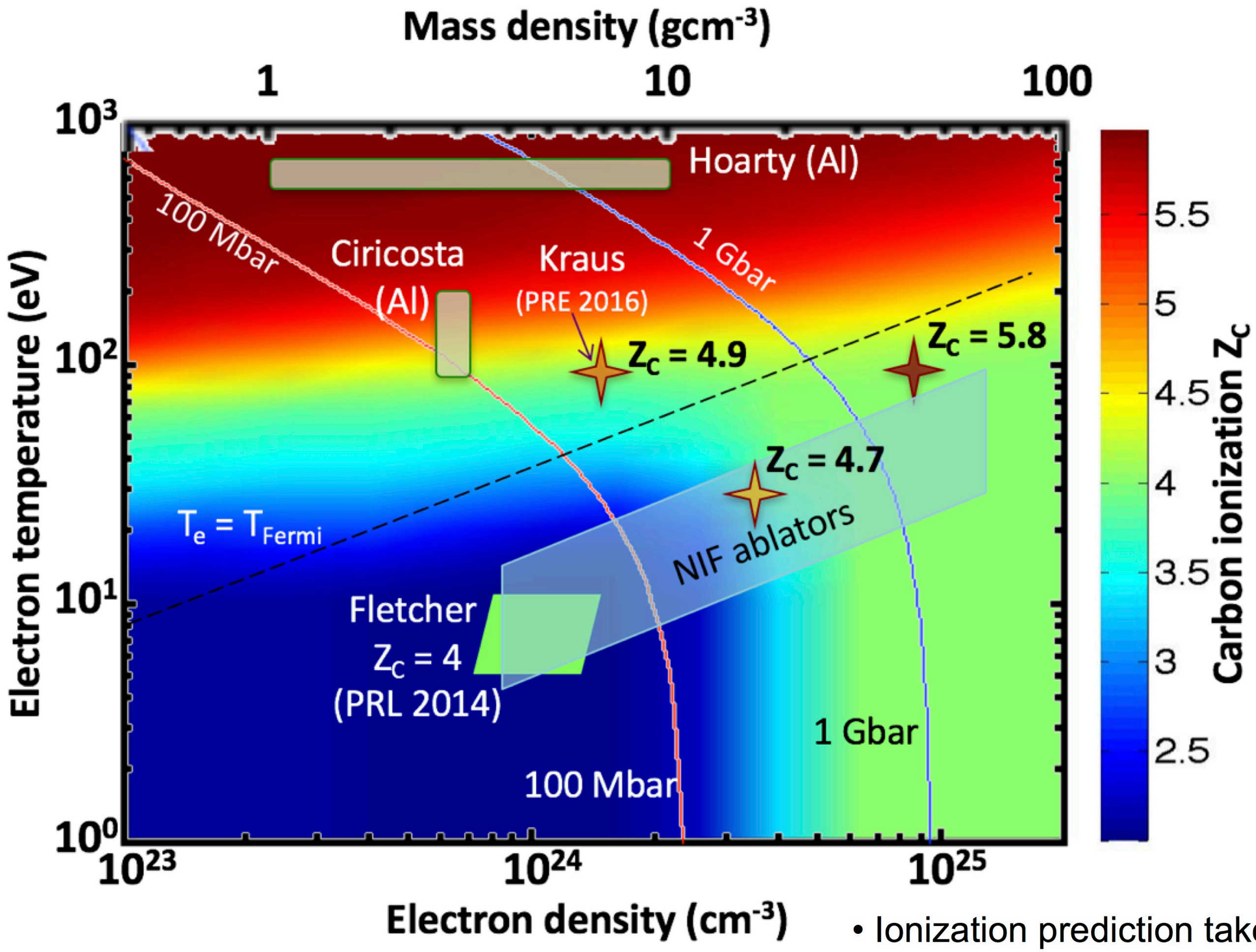

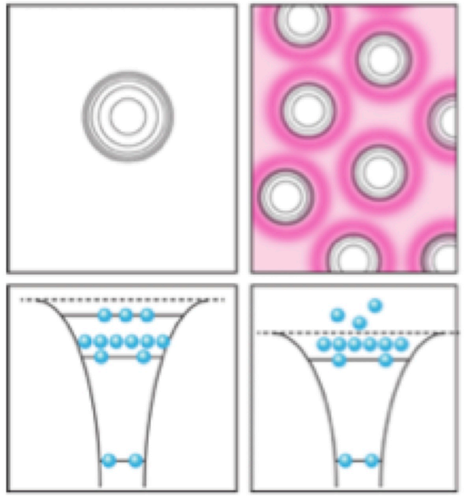

NIF data point

Hoarty et al., PRL **110**, 265003 (2013)

Ciricosta et al., PRL **109**, 065002 (2012)

Fletcher et al., PRL **112**, 145004 (2014)

Kraus et al., PRE **94**, 011202(R) (2016)
[C. Lin et al., PRE 96, 013202 (2017)]

- Ionization prediction taken from OPAL

Rogers et al., APJ **456**, 902 (1996)

Preliminary, from Tilo Döppner et al., LLNL

Ionization potential depression: correlation effects

- **ionization potential depression and structure factor**

$$\boxed{\Delta_{\mathrm{IPD}}^{\mathrm{ion-ion}} = -\frac{(Z_i+1)e^2}{2\pi^2\epsilon_0 r_{\mathrm{WS}}} \cdot f(\Gamma_i) \int_0^\infty \frac{dq_0}{q_0^2} S_{\mathrm{ii}}^{\mathrm{ZZ}}(q_0)}$$

$$f(\Gamma_i) = \frac{3\Gamma_i}{\sqrt{(9\pi/4)^{2/3} + 3\Gamma_i}}$$

- **results**

- low density (weak coupling): Debye-Hückel (DH)
- high density (strongly coupled): Ion sphere (IS) model
- transition from Stewart-Pyatt (SP) model to Ecker-Kröll (EK) model

C. Lin *et al.*, Phys. Rev. E **96**, 013202 (2017)

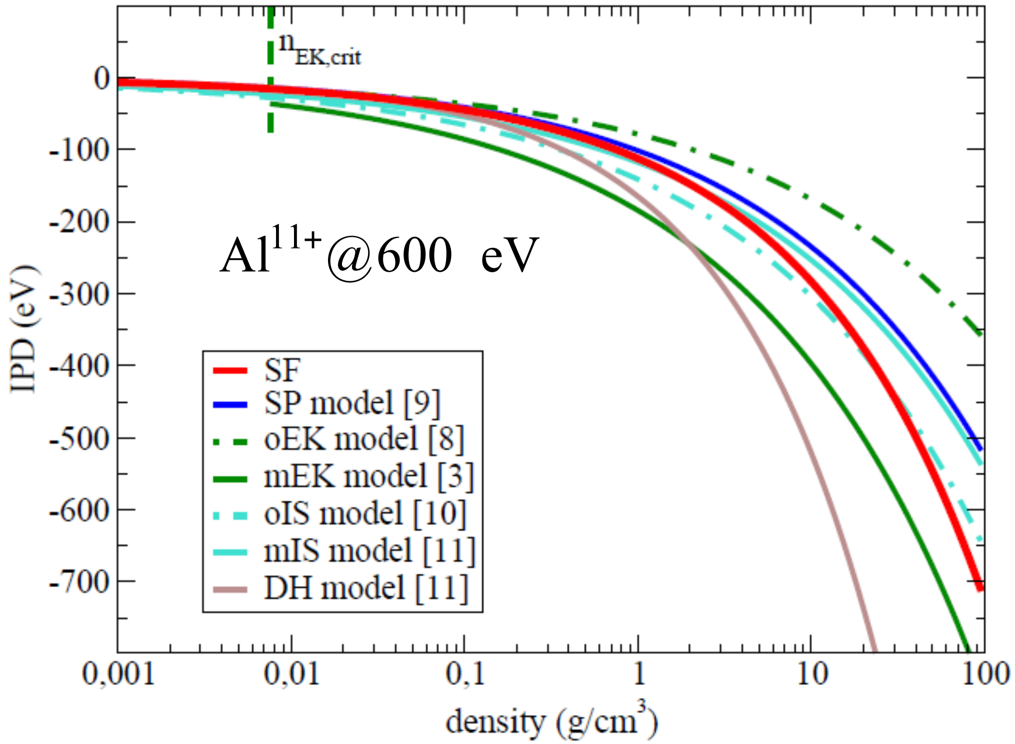

Pauli blocking – phase space occupation

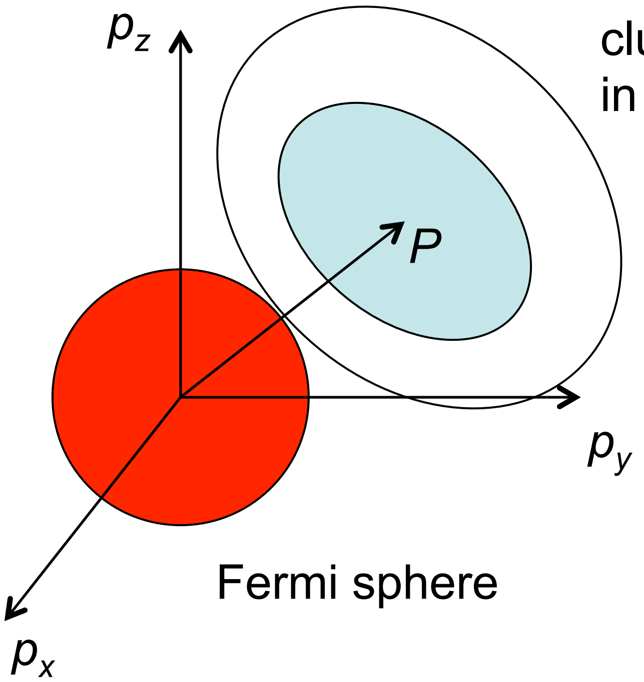

cluster wave function (atom, ions,…)
in momentum space

P - center of mass momentum

The Fermi sphere is forbidden,
deformation of the cluster wave function
in dependence on the c.o.m. momentum P

momentum space

The deformation is maximal at $P = 0$.
It leads to the weakening of the interaction
(disintegration of the bound state).

IPD of C^{5+} at T=100 eV

cf. talk by Khomkin A. L.

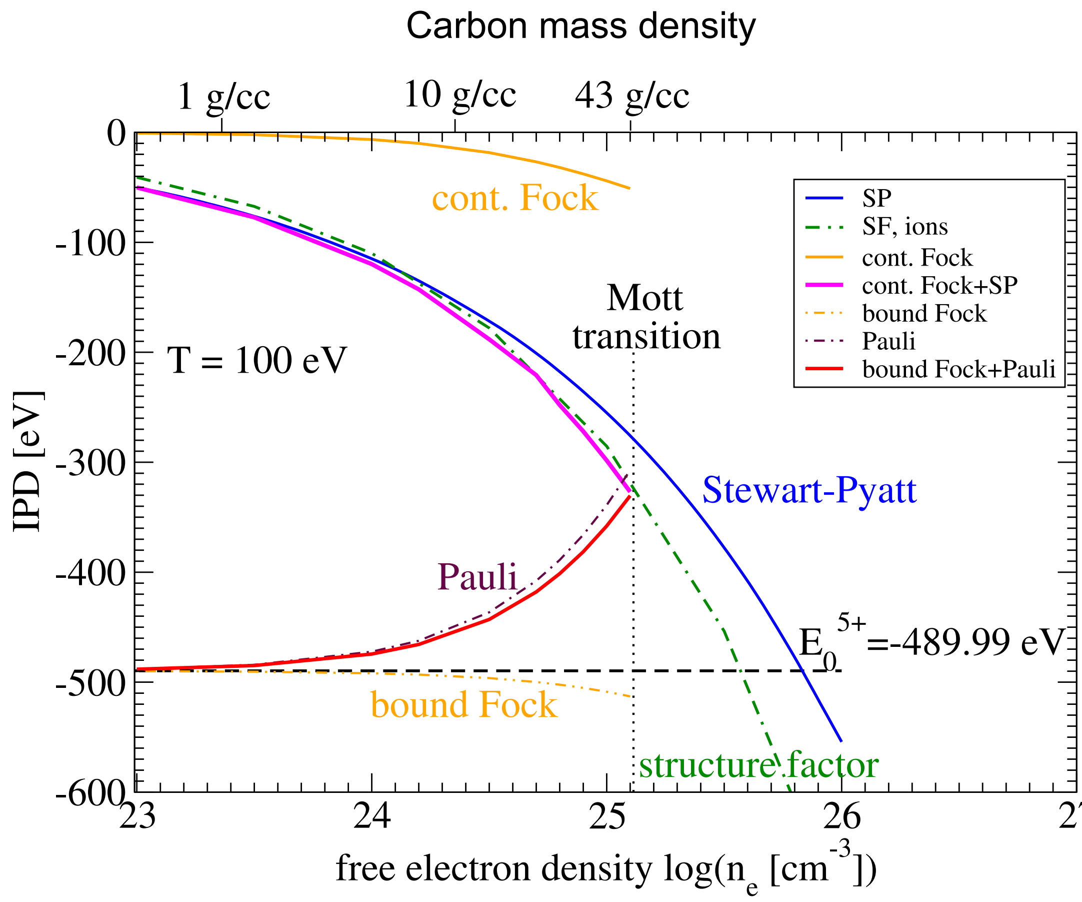

Stewart-Pyatt

ion structure factor

degeneracy:
Fock shifts
(continuum,
bound state),

and Pauli shift
(bound state)

G. Röpke, D. Blaschke, T. Döppner, C. Lin, W. D. Kraeft, R. Redmer, and H. Reinholz, Phys. Rev. E **99**, 033201 (2019).

Ionization degree of C plasmas

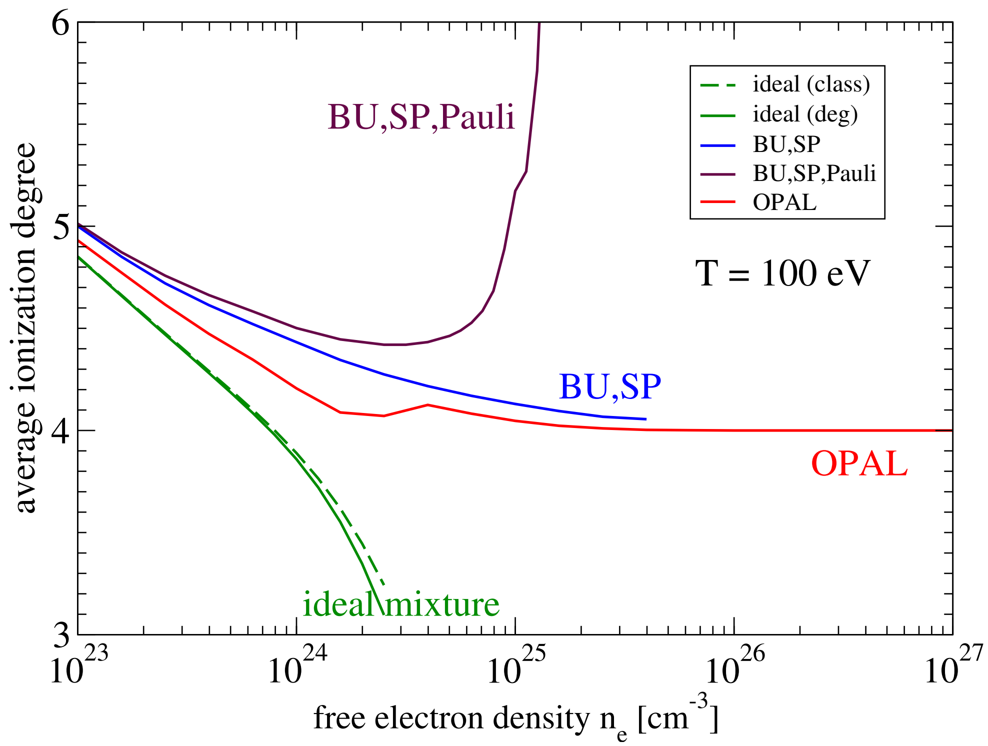

Stewart-Pyatt (SP)

OPAL

degeneracy:
Fock shifts
(continuum,
bound state),

and Pauli shift
(bound state)

partial densities
(BU)

$$\sigma_{C^{5+}}^{\text{bound}}(T) = \sum_{\gamma,\nu}^{\text{bound}} \left[e^{\beta I_{\gamma,\nu}^{5+}} - 1 \right] \theta\left(I_{\gamma,\nu}^{5+} \right), \qquad \theta(x) = \begin{Bmatrix} 1 & \text{if } x > 0, \\ 0 & \text{else,} \end{Bmatrix}$$

G. Röpke, D. Blaschke, T. Döppner, C. Lin, W. D. Kraeft, R. Redmer, and H. Reinholz,
Phys. Rev. E **99**, 033201 (2019).

Free electron density

Kubo-Greenwood formula: conductivity

$$\sigma^{\mathrm{tot}}(\omega) = \frac{2\pi e^2}{3\Omega\omega} \sum_{\mathbf{k}\nu\mu} (f_{\mathbf{k}\nu} - f_{\mathbf{k}\mu}) \left| \langle \mathbf{k}\nu | \, \hat{\mathbf{v}} \, | \mathbf{k}\mu \rangle \right|^2 \times \delta\left(E_{\mathbf{k}\mu} - E_{\mathbf{k}\nu} - \hbar\omega\right).$$

$$\sigma^{\mathrm{tot}}(\omega) = \sigma^{\mathrm{f\text{-}f}}(\omega) + \sigma^{\mathrm{b\text{-}f}}(\omega) + \sigma^{\mathrm{b\text{-}b}}(\omega)$$

Thomas-Reiche-Kuhn sum rule

$$Z^{\mathrm{tot}} = \frac{2m_e V}{\pi e^2 n_{\mathrm{i}}} \int_0^{+\infty} d\omega \; \sigma^{\mathrm{tot}}(\omega)$$

Ionization degree $Z^{\mathrm{free}}/Z^{\mathrm{tot}}$

$$Z^{\mathrm{free}} = \frac{n_{\mathrm{e}}^{\mathrm{free}}}{n_{\mathrm{i}}} = \frac{2m_e V}{\pi e^2 n_{\mathrm{i}}} \int_0^{+\infty} d\omega \; \sigma^{\mathrm{f\text{-}f}}(\omega)$$

Carbon, T = 100 eV, n = 50 g cm^{-3}

final sum rule values

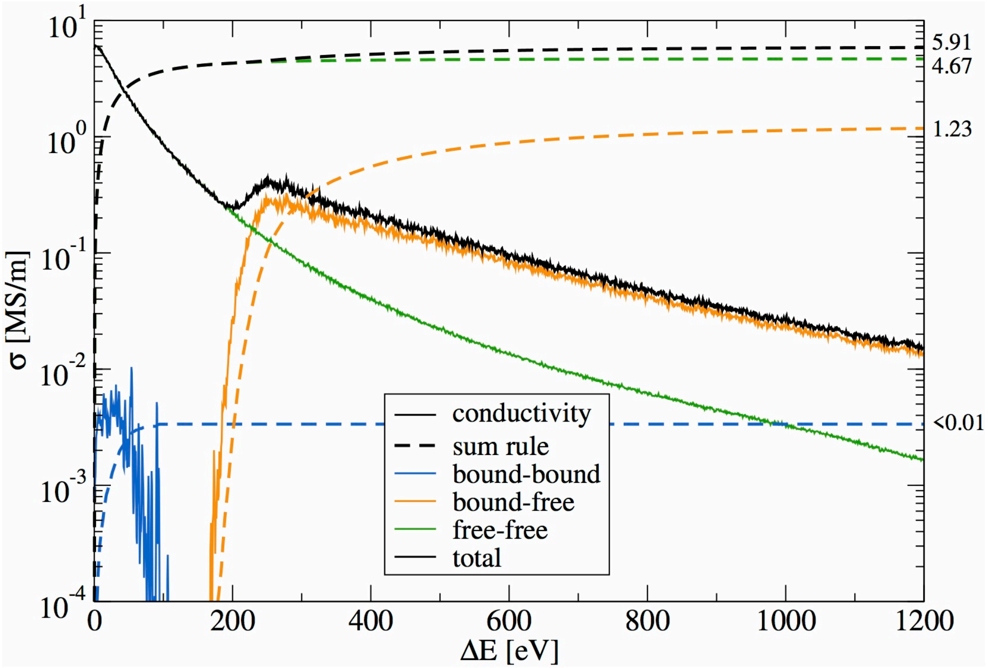

M. Bethkenhagen et al., Phys. Rev. Research 2, 023260 (2020)

Ionization degree for carbon

T = 100 eV

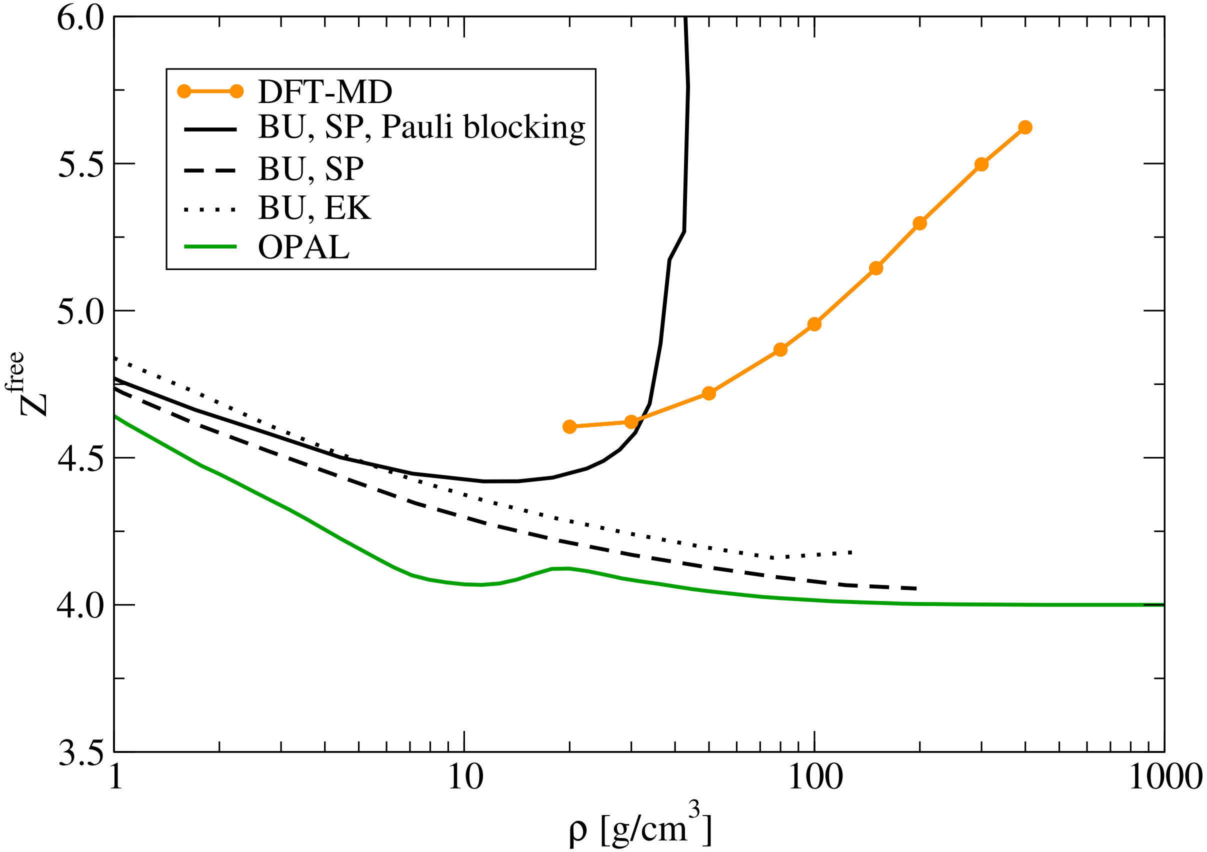

Ionization degree of carbon Z^{free} derived from DFT- MD simulations (orange line) compared to predictions of OPAL (green line) and Beth-Uhlenbeck (BU) calculations (black lines).

BU results incorporate the EK and SP models, respectively.

Solid line takes into account Pauli blocking effects in addition.

M. Bethkenhagen et al., Phys. Rev. Research 2, 023260 (2020)

DC conductivity of Al

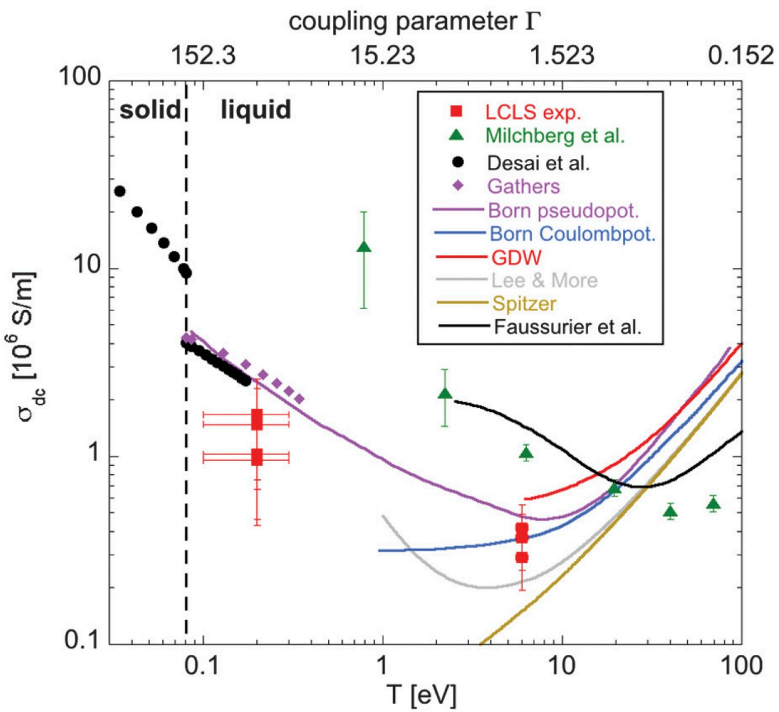

Thomson scattering at LCLS
(Linac Coherent Light Source)

Collisional-damped plasmons
in isochorically heated WDM

FIG. 4 (color). dc conductivity as a function of the temperature for a density of 2.7 g/cm^3 and an ionization degree of $Z_f = 3$. Extracted results of this work (red squares), experimental results of Desai *et al.* [15] (black dots), Gathers [18] (violet rhombus), and Milchberg *et al.* [20] (green triangles) as well as the theoretical models of Lee and More [24] (gray), Spitzer *et al.* [57] (gold), Faussurier and Blancard [29] (black), GDW [31] (red), and Born [58] (blue) are indicated (screened Coulomb interaction, no ion-ion correlation). To study the influence of the ion-ion structure factor and a pseudopotential [61], the dc conductivity with the corresponding Born collision frequency (Born improved, violet) is also shown.

P. Sperling *et al.*, PRL **115**, 115001 (2015)

Dynamic electrical conductivity

Ziman formula:
ion-ion structure factor S_{ii},
el. – ion scattering cross section $\Sigma(q,k)$

$$\frac{1}{\sigma} = \frac{\hbar}{3\pi Z e^2 n_e} \int_0^\infty d\varepsilon \, [-f'(\varepsilon)] \int_0^{2k} dq \, q^3 \, S_{ii}(q) \, \Sigma(q,k)$$

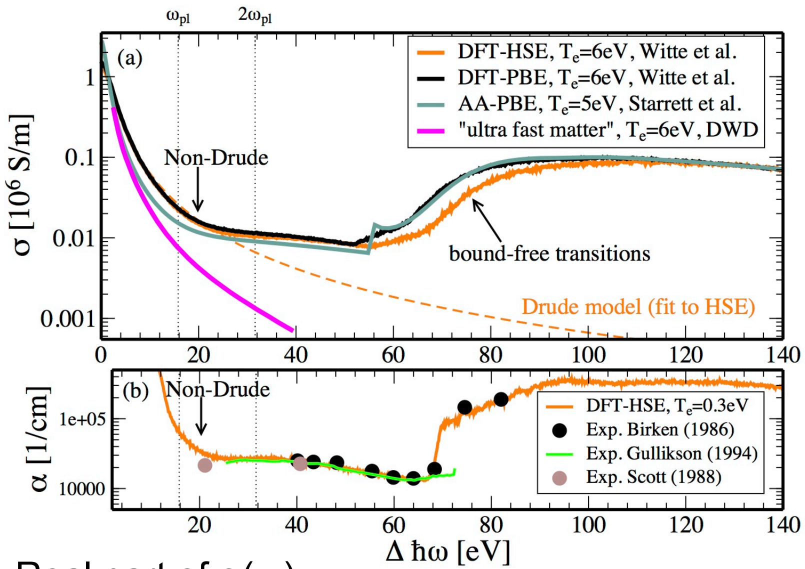

Real part of $\sigma(\omega)$
and absorption coefficient α of Al at 2.7 g/cm^3

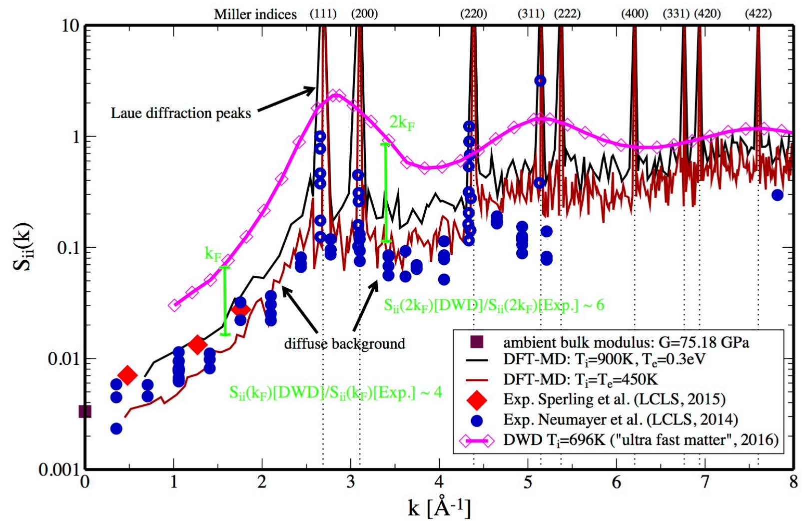

FIG. 1. $S_{ii}(k)$ of aluminum measured at LCLS by Sperling *et al.* [3] (red squares) and Neumayer *et al.* [8] (blue circles) within ultra-short 25-50 fs pulses in comparison with predictions of DWD [1] and DFT-MD.

Kubo-Greenwood formula

$$\lim_{k\to 0} \sigma(\omega) = \frac{2\pi e^2}{3\Omega\omega} \sum_{\mathbf{k}\nu\mu} (f_{\mathbf{k}\nu} - f_{\mathbf{k}\mu}) \, |\langle \mathbf{k}\nu | \hat{\mathbf{v}} | \mathbf{k}\mu \rangle|^2 \times \delta(E_{\mathbf{k}\mu} - E_{\mathbf{k}\nu} - \hbar\omega) \, .$$

$$\langle k_1 | \hat{\mathbf{p}} | k_2 \rangle = \hbar \mathbf{k}_1 \delta_{k_1,k_2} + \frac{\langle k_1 | \hat{V} | k_2 \rangle}{E_1 - E_2} (\hbar \mathbf{k}_1 - \hbar \mathbf{k}_2)$$

B. Witte, G. Röpke, P. Neumayer, M. French,
P. Sperling, V. Recoules, S. H. Glenzer, and R. Redmer, Phys. Rev. E **99**, 047201 (2019)

DC conductivity Al

Kubo-Greenwood formula, DFT-MD

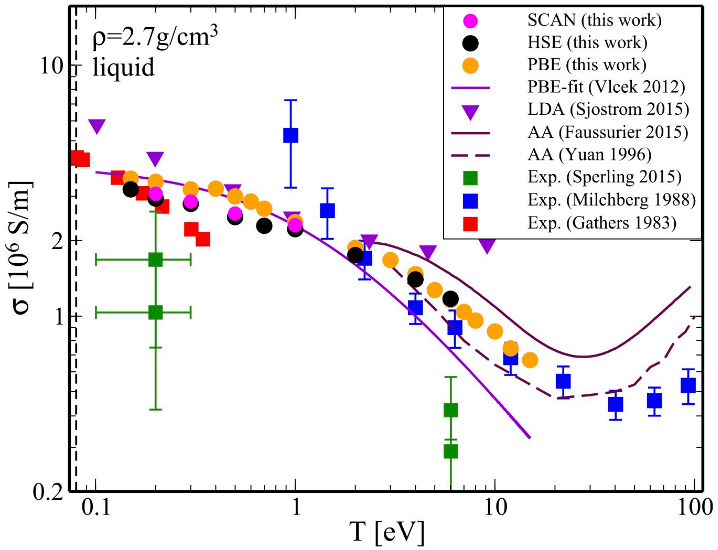

FIG. 8. DC conductivity for solid density aluminum as a function of temperature from DFT-MD simulations applying HSE (black circle), SCAN (purple circle), and PBE functional (orange circle). We compare our results to values from Sperling *et al.*,[9] Milchberg *et al.*,[85] Gathers[86] (density uncorrected for expansion, isochoric), Faussurier and Blancard,[87] and Yuan *et al.*[88] We also compare to DFT results from Sjostrom and Daligault (triangles).[84]

Witte *et al.*, Phys. Plasmas 25, 056901 (2018)

Quantum Landau-Fokker-Planck equation, mean-force scattering

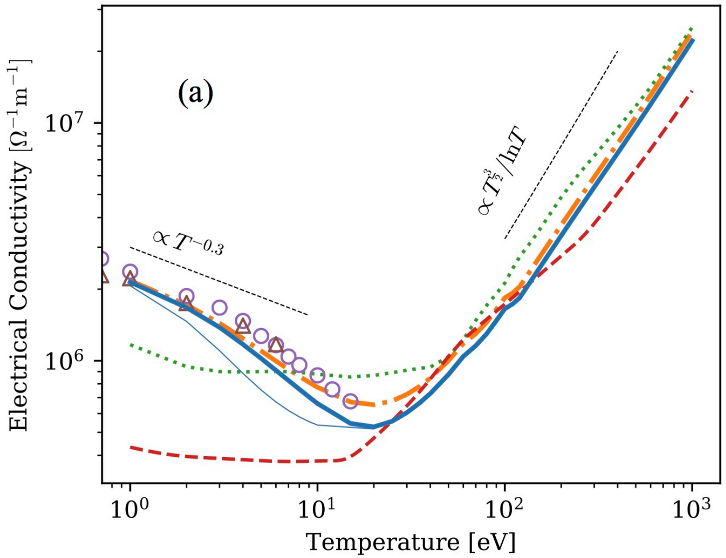

Electrical conductivity of solid-density aluminum plasma (ρ = 2.7g/cm³).
The circles and triangles are QMD data by Witte *et al.*
Dotted green curves : Lee-More model.
Dashed red curves: interpolations of Rinker's tables.

N. R. Shaffer and C. E. Starrett, Phys. Rev. E **101**, 053204 (2020)

Including electron-electron collision

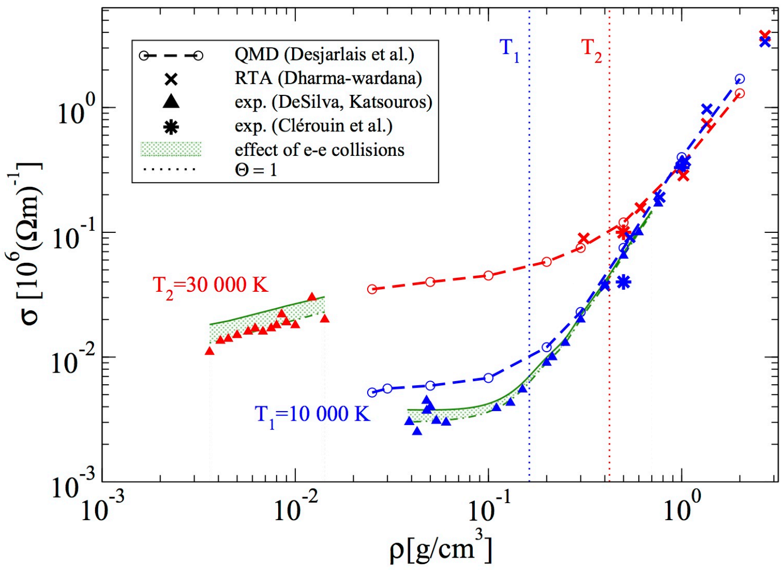

FIG. 2. (Color online) Aluminum dc conductivity as function of density for 10 000 K (blue) and 30 000 K (red). Experiments were performed by DeSilva and Katsouros [57] (triangles) and Clerouin *et al.* [56] (stars) for which regression curves are given by dashed-dotted lines (green). The DFT-MD results of Desjarlais *et al.* [20] are shown as hollow circles on dashed lines. Calculations of Dharma-wardana [4] based on the relaxation time approximation (RTA) are given as crosses. Degeneracy effects become important right to the vertical dotted lines ($\Theta = 1$). Solid lines (green) show the conductivity of a hypothetical Lorentz plasma, obtained by extracting the e-i scattering contributions from the regression curve (dashed-dotted line) according to the correction factor R_{ee}, Eq. (34), for the given densities and temperatures.

$$\sigma^{(L)}(\omega) = \frac{\epsilon_0 \omega_{\mathrm{pl}}^2}{-i\omega + r^{(L)}(\omega)\nu^{\mathrm{Ziman}}(\omega)}$$

$$r^{(2)}(0) = \frac{d_{33}d_{11} - d_{13}d_{31}}{d_{11}\left[d_{33} + \frac{N_{13}^2}{N_{11}^2}d_{11} - \frac{N_{31}}{N11}d_{13} - \frac{N_{13}}{N11}d_{31}\right]}$$

correlation functions $d_{ll'} = \frac{1}{3}\langle \dot{\hat{\mathbf{P}}}_l; \dot{\hat{\mathbf{P}}}_{l'}\rangle_{\omega+i\eta} = d_{ll'}^{\mathrm{ei}} + d_{ll'}^{\mathrm{ee}}$

$$L_{\mathrm{Zi}} = \frac{3\pi^{1/2}}{4}\Theta^{3/2}\int_0^\infty dq\; q^3 f_{\mathrm{e}}(q/2)\left|\frac{V_{\mathrm{ei}}(q)}{\epsilon_{\mathrm{e}}^{\mathrm{RPA}}(q,0)}\right|^2 \frac{\epsilon_0^2}{e^4} S_{\mathrm{ii}}(q)$$

$$R_{\mathrm{ee}}^{\mathrm{KT}} = \lim_{\Theta\gg 1}\frac{\sigma^{\mathrm{KT}}}{\sigma^{\mathrm{Lorentz}}} = \frac{0.591}{1.016} = 0.582$$

H. Reinholz *et al.*, Phys. Rev. E **91**, 043105 (2015)

Electron transport in dense plasmas

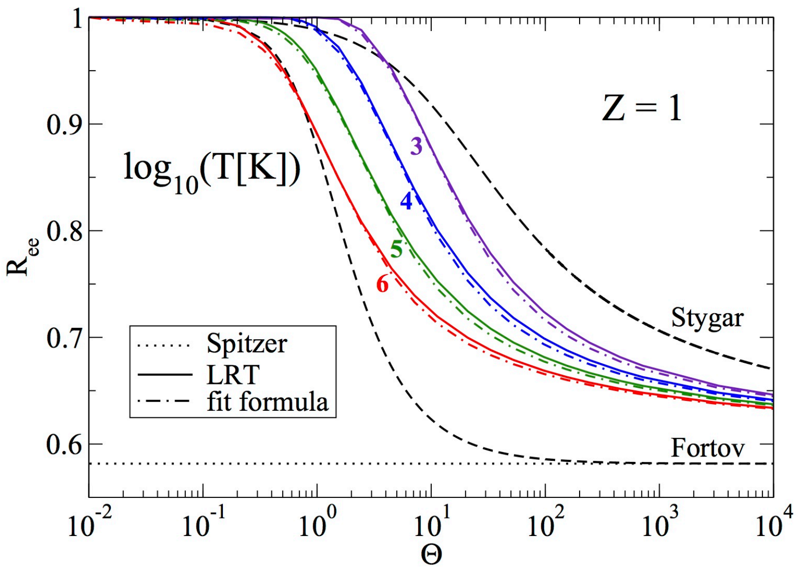

FIG. 1. (Color online) Correction factor R_{ee} of the conductivity due to e-e collisions as function of degeneracy parameter Θ at $Z = 1$ for different temperatures $T = (10^3, 10^4, 10^5, 10^6)$ K. Numerical calculations (LRT, full lines) are compared with the fit formula (34) (dot-dashed lines) and the approximations (40) of Stygar *et al.* [11] and (41) of Fortov *et al.* [12] (dashed lines).

and Fortov *et al.* [12],

$$R_{\mathrm{ee}}^{\mathrm{Fortov}}(\Theta,Z) = R_{\mathrm{ee}}^{\mathrm{KT}}(Z) + \frac{1 - R_{\mathrm{ee}}^{\mathrm{KT}}(Z)}{\sqrt{1+\Theta^2}}, \tag{41}$$

with the Spitzer values $R_{\mathrm{ee}}^{\mathrm{KT}}(Z=1) = 0.582$, see Eq. (29),

H. Reinholz *et al.*, Phys. Rev. E **91**, 043105 (2015).

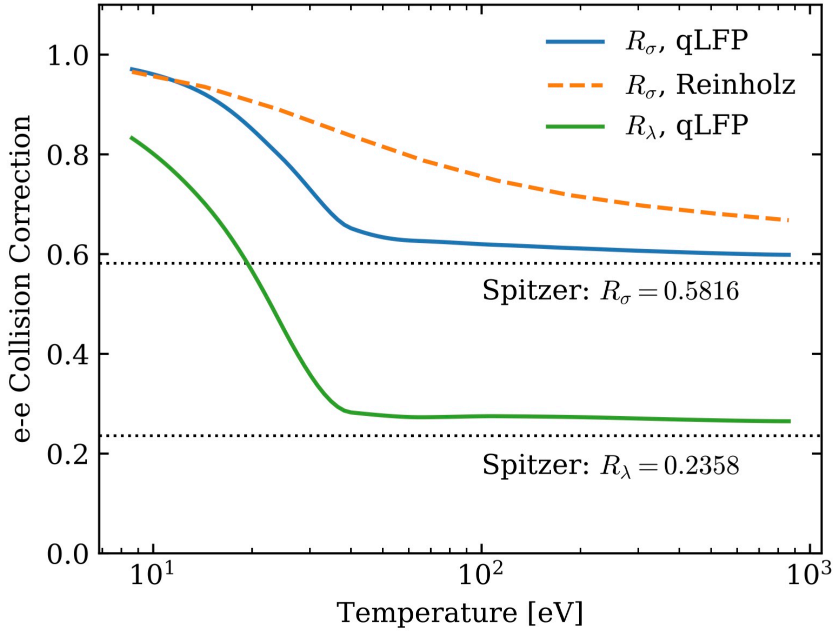

FIG. 6. Electron-electron correction factor to the electrical conductivity, R_σ, and thermal conductivity, R_λ, for compressed hydrogen at $\rho = 1\,\mathrm{g\,cm^{-3}}$. Solid blue and green lines are the present qLFP model. The dashed orange line is the practical formula by Reinholz *et al.* [10]. The dotted black lines are the Spitzer-Härm result [7].

Electron-electron collisions

N. R. Shaffer and C. E. Starrett, Phys. Rev. E **101**, 053204 (2020)

Conductivity of partially ionized plasmas

Contribution of electron-atom collisions
to the plasma conductivity of noble gases

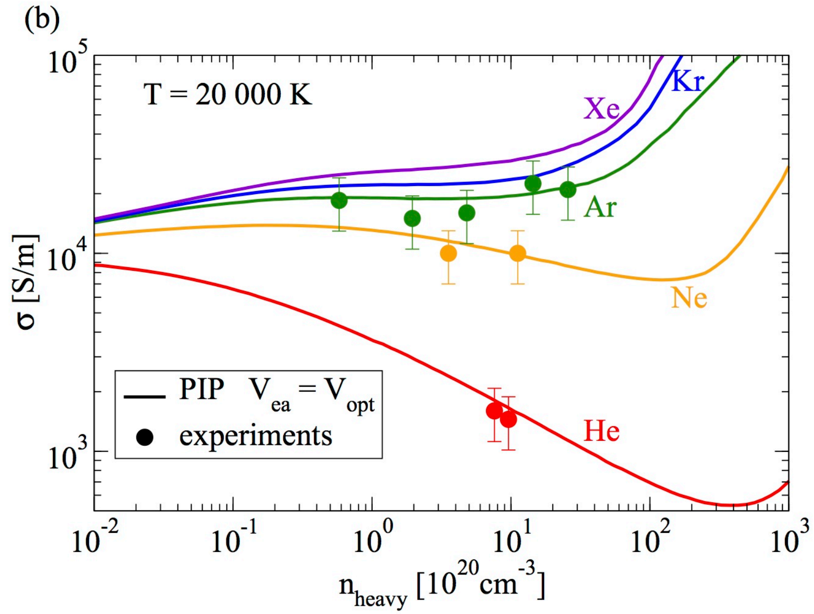

Conductivity of partially ionized noble gases (PIP)
using the optical potential for the e-a interaction
helium (red), neon (orange), argon (green),
krypton (blue), and xenon (violet) at 20 000 K
in comparison with experimental data

S. Rosmej, H. Reinholz, and G. Röpke,

Phys. Rev. E **95**, 063208 (2017)

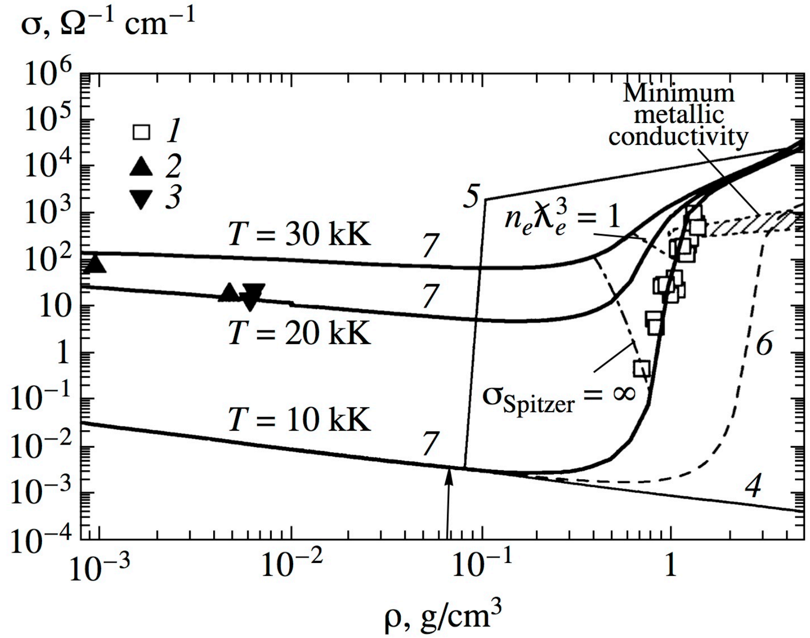

Fig. 9. Electrical conductivity of helium as a function of density: (*1*), (*2*), and (*3*) experimental data from [42], [57], and [61], respectively; (*4*) electrical conductivity calculated with the plasma composition corresponding to the model of an ideal plasma; (*5*) results obtained with the plasma composition calculated on the basis of the Debye–Hückel model [1]; (*6*) results obtained with the plasma composition calculated on the basis of the bounded-atom model [2, 22] featuring a fixed radius of the helium atom ($r_a = 1.3a_0$); and (*7*) results of the present study.

V. E. Fortov *et al.*, J. Exp. Theor. Phys. **97**, 259 (2003)

Conclusions

1. New experiments explore nonideal plasmas in the region of strong degeneracy (warm dense matter).

2. Ionization degree becomes problematic (definition? calculation?).
   Pauli blocking is responsible for pressure ionization at low temperatures.
   “cold” ionization (Khomkin)?-impurity problem?

3. To calculate the dynamical, frequency-dependent electrical conductivity, the electron-ion interaction can be treated systematically using the DFT approach. The account of the electron-electron interaction beyond the mean-field approximation remains an open problem.

4. The investigation of thermodynamic, transport and optical properties of different materials in the non-ideal plasma region remains an interesting field of research with relevance for laboratory experiments, technical applications and astrophysical phenomena.

Thank you for your attention

Density effects

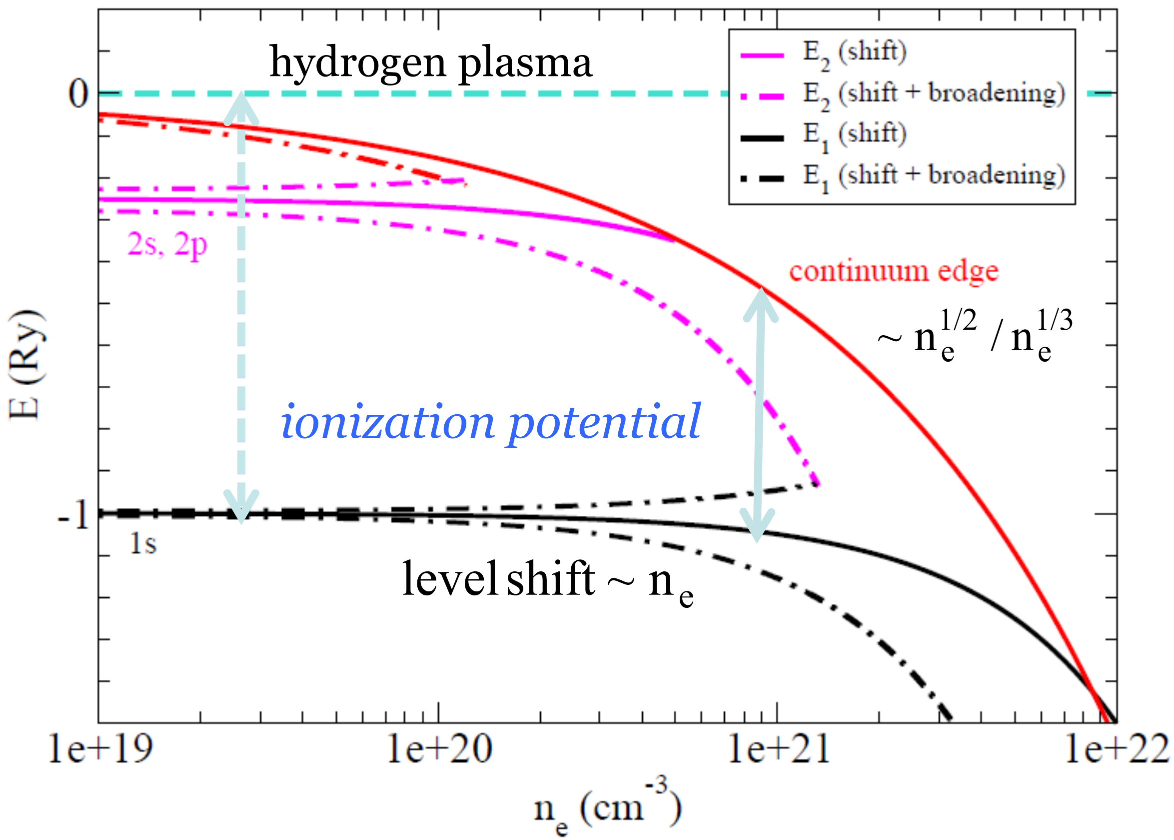

Experiments: high precision
semiconductors (el.-hole-exciton)
Warm dense matter (WDM)

- change of eigenenergy: continuum lowering, level shift

Debye shift
microfield

- Green functions
- QMD
- DFT

Simple theoretical approaches

- **low density limit: Debye-Hückel (DH) theory**

$$\boxed{\triangle I_{\mathrm{DH}} = \frac{Z_{\mathrm{ion}} e^2}{(4\pi\varepsilon_0)\,\lambda_{\mathrm{D}}}} \sim \mathrm{n}^{1/2}$$

inverse Debye length: $\lambda_{\mathrm{D}}^{-1} = \sqrt{\dfrac{e^2 \sum_i (z_i^2 + z_i) n_i}{\varepsilon_0 k_{\mathrm{B}} T_e}}$

W.-D. Kraeft, D. Kremp, W. Ebeling, and G. Röpke, Quantum Statistics of Charged Particle System, 1986

- **high density limit: Ion sphere (IS) model**

G. Zimmerman and R. More, JQSRT **23**, 517, 1980

$$\boxed{\triangle I_{\mathrm{IS}} = \frac{9}{5}\,\frac{Z^*\, e^2}{4\pi\varepsilon_0 R_{\mathrm{is}}}} \sim \mathrm{n}^{1/3}$$

Z^* : mean charge

R_{is} : ion sphere radius

$$\frac{4\pi\, R_{\mathrm{is}}^3\, n_{\mathrm{ion}}}{3} = 1$$

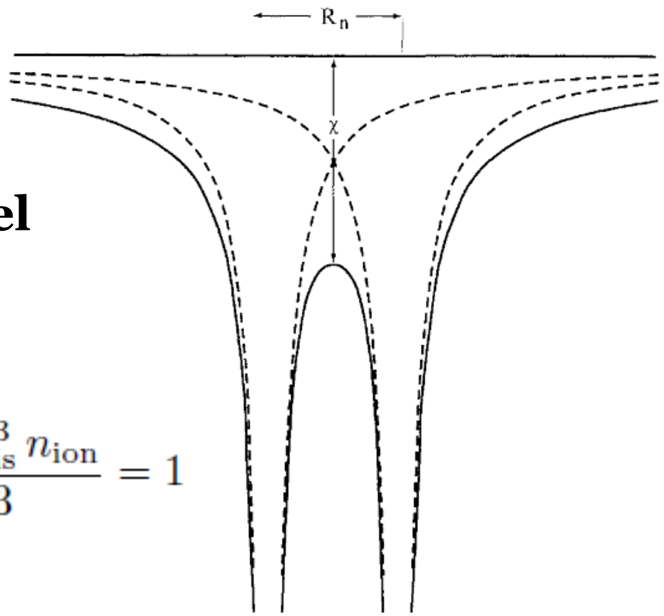

D. Salzmann, Atomic Physics in Hot Plasmas, 1998

Simple theoretical approaches

- **Stewart-Pyatt (SP) model** J.C. Stewart and K. D. Pyatt., Astrophys. J. **144**, 1203, 1966

$$\Delta I_{\mathrm{SP}} = \frac{3}{2} \cdot \frac{(Z_{\mathrm{ion}} + 1)e^2}{(4\pi\varepsilon_0)R_{\mathrm{is}}} \left\{ \left[1 + \frac{\lambda_{\mathrm{D}}}{R_{\mathrm{is}}} \right]^{2/3} - \left(\frac{\lambda_{\mathrm{D}}}{R_{\mathrm{is}}} \right)^2 \right\}$$

- **Ecker-Kröll (EK) model** G. Ecker and W. Kröll, Phys. Fluids **6**, 62, 1963

$$\triangle I_{\mathrm{EK}} = \begin{cases} (Z_{\mathrm{ion}} + 1)e^2 / (4\pi\varepsilon_0 \lambda_{\mathrm{D}}) & \text{if } n < n_{\mathrm{cr}} \\ C_{\mathrm{EK}} (Z_{\mathrm{ion}} + 1)e^2 / (4\pi\varepsilon_0 r_0) & \text{if } n \geq n_{\mathrm{cr}} \end{cases}$$

$$n_{\mathrm{cr}} = \frac{3}{4\pi} \left(\frac{k_{\mathrm{B}} T_e}{Z^2 e^2} \right)^3, n = \frac{N}{V}$$

$$r_0 = \sqrt[3]{\frac{3V}{4\pi N}}, \quad N = N_e + \sum_{\text{ion species}} N_{\mathrm{ion}}$$

In-medium Schrödinger equation

Consistent treatment of the two-particle problem:
in-medium wave equation

$$\frac{p^2}{2m_e}\psi_n(p)+\sum_q V(q)\psi_n(p+q)-E_n\psi_n(p)=\sum_q V(q)\left[\psi_n(p+q)f_e(p)-\psi_n(p)f_e(p+q)\right]$$

Pauli blocking, Fock self-energy shift, Fermi fct. f_e

V(q) --> dynamically screened Coulomb interaction

$$V^{\mathrm{s}}_{ab}(q,\omega)=V_{\mathrm{ab}}(q)\cdot\left\{1+\int\frac{d\bar{\omega}}{\pi}\cdot\frac{\mathrm{Im}\,\varepsilon^{-1}(q,\bar{\omega}-i\eta)}{\omega-\bar{\omega}}\right\}$$

dynamical screening, dynamical self-energy

$\epsilon(\mathbf{q},\omega+i0)$ dielectric function

R. Zimmermann, K. Kilimann,
W. D. Kraeft, D. Kremp and G. Röpke
Phys. Stat. sol. (b) **90**, 175 (1978)

W.-D. Kraeft, D. Kremp, W. Ebeling, G. Röpke
Quantum Statistics of Charged Particle Systems,
Akademie-Verlag, Berlin 1986